



# Wear resistance and friction analysis of Ti6Al4V cylindrical ball-burnished specimens with and without vibration assistance

Eric Velázquez-Corral<sup>1</sup> · Vincent Wagner<sup>2</sup> · Ramón Jerez-Mesa<sup>1</sup> · Karl Delbé<sup>2</sup> · Jordi Llumà<sup>3</sup> · J. Antonio Travieso-Rodríguez<sup>1</sup> · Gilles Dessein<sup>2</sup>

Received: 25 September 2022 / Accepted: 13 January 2023  
© The Author(s) 2023

## Abstract

The objective of the research is to analyze the impact of the ultrasonic vibration assistance on the wear resistance due to the topography enhancement caused on Ti6Al4V cylindrical samples after surface modification through a ball burnishing process. The process parameters considered for this study are the burnishing force, the number of passes, and the addition of a 40 kHz ultrasonic assistance, which are thought to enhance the surface topography and increase the hardener effect in terms of depth. A complete screening design of 3 factors was performed, revealing that the number of passes and the vibration assistance are the most important parameters for minimizing the wear volume loss, being 170 N of burnishing force, 3 passes, and the addition of the vibration assistance as the best combination found. However, no significant difference in the friction force was observed. The topography results show that there is a decrease in the average roughness from 1.50 to 0.45  $\mu\text{m}$  with optimal burnishing conditions. It was also analyzed the microstructure originated after the turning, the conventional ball burnishing, and the vibration-assisted ball burnishing, being the last optimal in terms of depth affectation to the microstructure. Therefore, these results confirm an improvement in terms of wear enhancement, friction reduction, and topography results when vibration assistance is added to a conventional ball burnishing process.

**Keywords** Vibration-assisted ball burnishing · Ball burnishing · Tribology · Microstructure analysis

## 1 Introduction

Titanium alloys have increasing importance in biomedical and engineering applications, such as in the aerospace, marine, or automotive industry. However, despite being materials with a good combination of mechanical properties and corrosion resistance, different researchers have highlighted that their tribo-characteristics are detrimental due to their high chemical reactivity with environmental materials [1, 2].

Due to this fact, several processes to modify the mechanical properties or the microstructure are used, like thermal oxidation [3, 4], cryogenic treatments [5, 6], or heat treatments like the nitriding [7] or annealing [8], to increase the hardness of the treated surface and reduce the friction [9]. However, despite being efficient processes in terms of wear enhancement, it has been reported a low depth of affectation where thermal oxidation is applied and surface roughening was reported for thermal treatments like nitriding.

Also, some mechanical treatments like the shot peening [10] have been used to modify the surface and test its tribo-characteristics, concluding that there is an improvement in the wear resistance due to the hardness increase measured, but degrading the surface roughness. Another common process to enhance the mechanical properties, like the external hardness, is the ball burnishing (BB) [1]. Ball burnishing is a cold deformation process in which the external surface of the workpiece treated is compressed by the application of a rolling ball, producing a smoother and hardened surface while not modifying dimensions [11]. This process could be able to improve the resistance to wear, reduce the coefficient

✉ J. Antonio Travieso-Rodríguez  
antonio.travieso@upc.edu

<sup>1</sup> Mechanical Engineering Department, Universitat Politècnica de Catalunya, Av. Eduard Maristany 10-14, 08019 Barcelona, Spain

<sup>2</sup> Laboratoire Génie de Production, École Nationale d'Ingénieurs de Tarbes, 47 Avenue d'Azereix, Tarbes, 65000 Occitanie, France

<sup>3</sup> Material Science and Metallurgical Engineering Department, Universitat Politècnica de Catalunya, Av. Eduard Maristany 10-14, 08019 Barcelona, Spain

of friction (by minimizing the adhesion of the two contacting surfaces), and prevent corrosion and oxidation in some cases. The process workflow can be divided into subsequent and simultaneous steps that result in an elastoplastic flow of the material, namely, the pile-up effect observed around the indenter during the burnishing process, which is mainly influenced by the work hardening of the material and the pressure exerted during the burnishing process, and the residual sink-in effect on the burnishing passage, having a great influence on the final surface morphology. In terms of wear enhancement, Revankar et al. [12] concluded that when the ball-burnishing process was applied to cylindrical Ti-6Al-4 V parts, the wear rate was decreased by 52% and the coefficient of friction by a 64% compared to conventional turned surface. Furthermore, he confirmed that the burnishing force and the number of passes were the most significant parameters, while the surface roughness and the external surface micro-hardness were improved. More recently, Attabi et al. [13] analyzed the wear enhancement of 316L stainless steels after a ball burnishing process, noticing that the number of passes is the most effective parameter in order to increase the depth of the deformed micro-structured layer and, therefore, having an influence on the frictional behavior. It was demonstrated that the wear loss can be optimized up to 65.2% and micro-hardness to 38.3% using one pass, compared with the core material.

In recent years, ultrasonic assistance has been introduced into super-finishing processes such as machining [14], laser cladding treatments [15], shot peening [16], magnetic abrasive finishing [17], or burnishing [18]. Particularly, since the 2010s, the tendency of using this technology in ball burnishing processes became really popular [19, 20]. The main line of investigation carried out by several authors is the topography enhancement of aluminum, carbon steel, or titanium alloys after the vibration-assisted ball burnishing process [21–24]. Jerez-Mesa et al. [25] performed a surface analysis of ball-end milled Ti-6Al-4 V and concluded that vibration assistance must be recommended to enhance the topography and the external hardness of the workpiece as long as the original surface has a Gaussian material distribution and with an Sq value of fewer than 5  $\mu\text{m}$ , but having no influence in terms of residual stresses. Teimouri et al. [26] concluded that the ultrasonic vibration power had the greatest impact among all the factors in terms of surface roughness and hardness in aluminum 6061's workpieces. These contributions can be related to the affirmation of Liu et al. [27], concluding that the vibratory effect of the ultrasonic assistance causes

local severe deformation having a major influence on the microstructure of the workpiece, obtaining a deeper effect in terms of hardness and a topography enhancement. In terms of wear enhancement and friction reduction, Velázquez-Corral et al. [28] concluded that the vibration-assisted ball burnished improves the wear by 15.9% and reduced the friction by 39.4% compared to conventional ball burnishing.

The aim of this present work is to investigate the contribution of the vibration assistance, within a ball burnishing process, on Ti6Al4V cylindrical samples in terms of topography, wear resistance, friction reduction, and depth of affectation on the microstructure. A final comparison between conventional ball burnishing and vibration-assisted ball burnishing is shown.

## 2 Materials and methods

### 2.1 Materials and first turning

Fifteen-millimeter diameter laminated bars of titanium alloy Ti-6Al-4 V were used for the experiments. The chemical composition of this material is shown in Table 1.

The machining and finishing processes were performed in 3-axis CNC Machine Lathe Pinacho SE 200  $\times$  750. All tests were performed with a constant cutting tool geometry, the cutting speed was 60 m/min, and the feed rate was 0.20 mm/rev. The resultant specimen was a 13-mm diameter. All specimens with an initial average roughness of  $1.5 \pm 0.2 \mu\text{m}$  were considered valid to be included in the experiments to restrict the variability of original surfaces and be able to compare the results obtained on every specimen. This will also be useful to notice the final roughness difference when the different ball-burnishing combinations are applied. Specimens whose initial roughness was out of that range were discarded to homogenize the original state of the treated materials.

### 2.2 Ball burnishing equipment and specimens

The tool used for this investigation is attached to a lathe. It is composed of a base armor, an ultrasonic actuation unit, a preload force unit (calibrated spring based on Hooke's law), and a working head, formed by one 10-mm and seven 2-mm diameter 100Cr6 chromium steel balls, the bigger one the contact ball with the treated surface (see Fig. 1). The ultrasonic actuation module is attached to a 40-kHz wave generator; the inner ceramic piezoelectric gets excited and

**Table 1** Chemical composition of Ti-6Al-4 V titanium alloy

Material	Chemical composition by element in wt%									
Ti6Al4V	Ti	Al	V	Fe	O	C	N	Y	H	
	Bal	6.10	4.00	0.25	0.20	0.0	0.01	0.001	0.001	

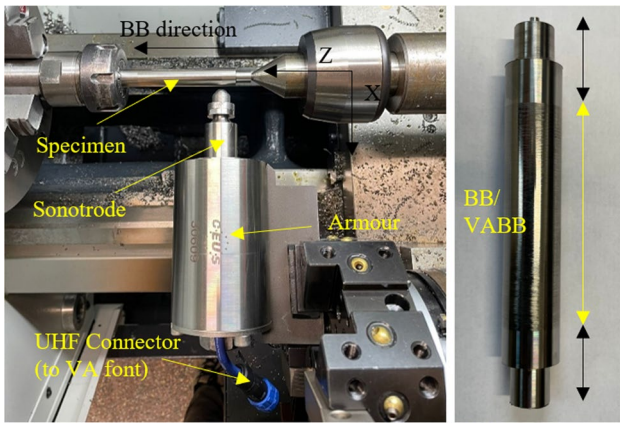


Fig. 1 Ball-burnishing tool and Ti6Al4V tribology sample

enters into a resonance mode, generating the movement of the sonotrode with an amplitude of vibration of 8  $\mu\text{m}$ .

The ball-burnishing force applied onto the specimen surface is the summary of the force based on a calibrated spring lodged, the ultrasonic vibratory force (when it is applied), and the low-frequency force variations due to the surface irregularities during the feed movement of the tool.

### 2.3 Experimental campaign and test specifications

The design of experiments was created according to a screening design of three burnishing parameters. This kind of DoE (*Design of Experiments*) is really helpful to reduce the total number of runs and screens out those variables that are not statistically significant. The input parameters are as follows:

- Burnishing force: three different levels, from 130 to 210 N with a central point in 170 N.
- Number of passes: three different levels, from 1 to 5 passes with a central point in 3 passes.
- Vibration assistance: two different levels, added or not with a frequency of 40 kHz.

The resultant combination is derived in a total of 12 different samples with a repetition of 2 random samples from the group, which is mandatory to complete the design of experiments (see Table 2). In addition, the burnishing speed and the burnishing feed were constant parameters, being 2 m/min (translated into 50 rpm of spindle speed) and 0.15 mm/rev, respectively.

In this experimental campaign, it is desired to test over the cylindrical resultant surface and determine the tribological characteristics, in terms of friction reduction and wear enhancement. However, the effect of the different burnishing parameters on these specimens needs a new variation of testing from the traditional pin-on-disk or pin-on-roll, mainly cause the best

Table 2 Design of experiments applied to treat the Ti-6Al-4 V alloy

Sample	Fb (N)	np	f (kHz)	Nomenc
1	170	5	40	170-5-40
2	130	3	0	130-3-0
3	210	1	0	210-1-0
4	210	5	0	210-5-0
5	170	3	40	170-3-40
6	210	5	0	210-5-0
7	170	1	0	170-1-0
8	130	5	0	130-5-0
9	130	5	40	130-5-40
10	130	1	40	130-1-40
11	210	1	40	210-1-40
12	130	1	40	130-1-40
13	210	3	40	210-3-40
14	170	3	0	170-3-0

strategy to test this new surface is perpendicular to the peaks and valleys and, therefore, parallel to the generatrix of the specimen and following a linear displacement. The equipment used for the tribology testing is a UMT TriboLab by BRUKER with the configuration presented in Fig. 2.

In order to define the tribology test parameters, it was followed the ASTM G132-96 “Standard Test Method for Pin Abrasion Testing” and Velázquez-Corral et al. previous work [28]. This standard covers the procedure to obtain the wear resistance by weighting the samples before and after the test and converting that mass loss into volumes. Wear is directly dependent on the mechanical characteristics of both materials (ball and abrasive surface) such as Young’s modulus, the Poisson’s ratio, and, in addition, the load applied that will define the worn print, which is defined by the Hertz contact law for indentations. The testing conditions are defined in Table 3.

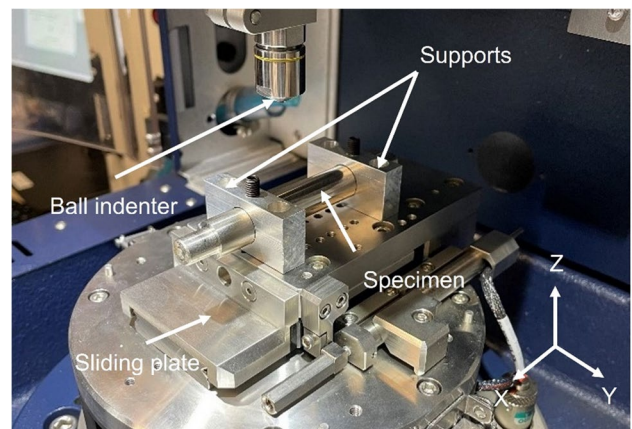


Fig. 2 Tribology setup for the new customized test

Once the tests have been performed, in order to determine the *cof* (coefficient of friction), it was tracked the value with a sampling frequency of 100 Hz, later filtered with a low-pass filter, and then, the average of the steady-state acquisition was calculated. For the wear measurement, it was measured the surface volume before and after each test, using the 3D non-contact profilometer Alicona InfiniteFocus with a 0.88 nm of resolution. The two surfaces were superposed and, therefore, the volume difference was calculated.

## 2.4 Phenomenology of the tribology test

In order to understand the phenomenology that is inside a wear process, Berthier, Godet and Denape et al. [29–31] proposed three conceptual tools: the tribological triplet (description of the system), the accommodation mechanisms (sites and modes of displacement's operating mechanisms), and the tribological circuit (dynamic view of the particle flow moving through the contact zone). These models are taken as a reference and a starting point to understand in depth how the interaction of the ball with the burnished surface happens during wear tests.

Firstly, the tribological triplet is divided into three different levels which define the test. The working device is the testing machine, in this case, the tribometer, which imposes the operation conditions and the mechanism's stiffness and corresponds to the first level. The second level is the two-contacting material (the Ti6Al4V specimen and the WC–Co ball) being the kind of contact geometry one of the dominating factors. Lastly, the inter-facial elements separate both surfaces and explain the local behavior of the contact in terms of particle adhesion [21].

Secondly, the accommodation mechanisms are defined in sites and modes. The sites correspond to the working device  $S_0$ , the contacting materials as  $S_1$  and  $S_2$ , the third body volume, originated due to the material transfer between the two bodies, as  $S_3$  and the superficial parts of this as  $S_4$  and  $S_5$ . The modes correspond to the fracture mechanics and material

behavior, being the elastic deformation  $M_0$ , the plastic deformation  $M_1$ , the fracture  $M_2$ , the shearing  $M_3$ , and the rolling mode  $M_4$ . The schema of this set-up is described in Fig. 3.

Thirdly, the tribological circuit helps to understand how the material is balanced and how flows during the test, in this case, will be analyzed the pile-up formed in the second body due to that material pushing to the laterals of the track.

Another very important factor to track is the quantity of oxygen that is present over the third body and the contacting materials' surfaces, due to the possible appearance of Fe-oxides or Ti-oxide, which will completely change the mechanical properties of this new layer and, therefore, a possible interaction in the resultant accommodation modes. For that, an energy-dispersive X-ray spectroscopy (EDS) analysis will be held over the  $S_2$  and  $S_4$  surfaces to perform a chemical characterization analysis.

## 2.5 Topography acquisition and measurement

The resulting surfaces prior and after the tribology test were acquired with a non-contact 3D profilometer ALICONA Infinite Focus G5, which allows the surface to be acquired by an adaptative focus of a set of lenses that assigns a certain height to the focal distance at that point.

The topographical parameters analyzed, for the prior surface, in this investigation are the amplitude parameters specified in the standard ISO 25178, namely,  $S_a$  (represents the arithmetical deviation of the roughness profile of the sampling length),  $S_q$  (the standard deviation of the heights), and  $S_{sk}$  and  $S_{ku}$  (distribution of the material at different heights on the surface). Skewness,  $S_{sk}$ , is a measure of the asymmetry of the profile about the mean line. Negative skewness indicates that a greater percentage of the profile is above the mean line and a positive value indicates that a greater percentage is below the mean line. The profiles with peaks removed or deep scratches have negative skewness, whereas profiles with valleys filled in or high peaks have positive skewness [32]. Kurtosis,  $S_{ku}$ , values higher than 3 represent abrupt surfaces, while values lower than 3 represent smoother surfaces. The data filtering used was done by eliminating the cylindrical surface, the atypical values, and a Gaussian noise-filtering.

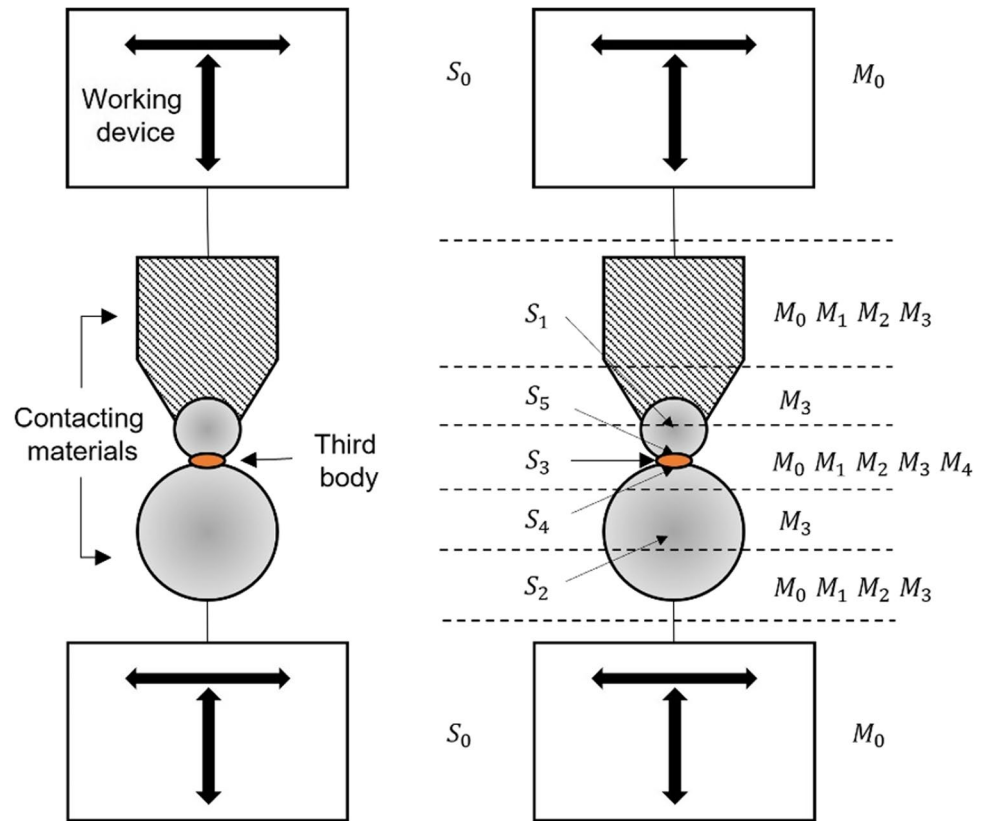
## 2.6 Microstructure and EDS analysis

Finally, scanning electron microscopy (SEM) analysis was done in order to see the microstructure evolution of the material for different burnishing conditions and an EDS to analyze the contact surfaces after the tribology testing, using an EVO HD15 by ZEISS equipped with an energy-dispersive X-ray spectrometer (SEM–EDX). Typical working parameters were an accelerating voltage of 15 kV, and a working distance of 10 mm.

**Table 3** Testing input parameters for the tribometer

Magnitude	Value	Units
Input load applied	20	N
Length of the print	20	mm
Ball material	WC–Co	-
Ball diameter	6	mm
WC–Co Young's modulus	600	GPa
WC Poisson's ratio	0.22	-
Ti6Al4V Young's modulus	120	GPa
Ti6Al4V Poisson's ratio	0.31	-
Time per test	5	min
Longitudinal speed	10	cm/s

**Fig. 3** Tribological triplet and accommodation mechanisms schematic



### 3 Results

#### 3.1 Topography of burnished surfaces

The original roughness for all samples was fixed to an initial average of  $1.5 \pm 0.2 \mu\text{m}$ , and the burnishing conditions applied are shown in Table 2. As was expected, all the specimens obtained better results in terms of average roughness than the original topography. The ratio of  $Sa/Sq$  kept similar for all the samples (around 0.8), which indicates the stability of this process in terms of topological parameters, independently of the burnishing conditions used. Also, the volume parameters were significantly improved, resulting in an almost perfect Gaussian distribution of material. The results are shown in Table 4.

In terms of average roughness enhancement, the bests results obtained correspond to the samples 210–3–40 (with a maximum value of 70%), 170–5–40, and 170–3–40, which have in common the addition of the vibration assistance plus a medium–high level of burnishing force and number of passes. More specifically, if burnishing force plus the number of passes equal pairs are compared in order to see the effect of the vibration assistance, it is seen that the vibration assistance has a positive effect. This can be explained by comparing the samples 130–5–0 vs 130–5–40, 210–1–0 vs 210–1–40, or 170–3–0 vs 170–3–40 (pairs that have the same burnishing force and the number of passes); all these

**Table 4** Topography results for each specimen

Nomenc	$\Delta Sa/Sa'$ (%)	$Sa/Sq$	Ssk	Sku
130–1–40	56	0.806	0.310	2.836
130–3–0	50	0.809	0.139	2.629
130–5–0	60	0.783	–0.140	3.365
130–5–40	61	0.799	0.099	2.882
170–1–0	55	0.782	0.331	3.437
170–3–0	58	0.782	0.293	3.279
170–3–40	64	0.801	0.071	2.784
170–5–40	67	0.800	0.213	3.017
210–1–0	52	0.793	0.174	3.160
210–1–40	62	0.807	0.066	2.674
210–3–40	70	0.759	0.082	4.034
210–5–0	55	0.798	0.229	2.883

combinations show an improvement around 6–10% in favor of the vibrated-assisted ball burnishing specimens, confirming the improvement in terms of resulting roughness.

However, for the material distribution, parameters did not found any special relation to the burnishing inputs. All values reported are close to the considered optimal, following a Gaussian distribution with Ssk equal to 0 and Sku equal to 3, obtaining smooth surfaces with almost every burnishing combination tried.

### 3.2 Effect of the VA on the final microstructure

The microstructures shown in Fig. 4 correspond to a cross-sectional part of samples 8 (130–5-0) for ball burnishing (BB) and 9 (130–5-40) for vibration-assisted ball burnishing (VABB). It also extracted a non-burnished sample section in order to do the comparison between the three resultant microstructures. The general images (see Fig. 8, 1st row) show a perspective of  $\beta$ -grains over an  $\alpha$  matrix, which defines the general microstructure of these Ti6Al4V specimens.

The images display a shearing and compression effect on the phase  $\alpha/\beta$  near the surface. As it can be seen, depending on the process performed, the depth of affectation varies from 2 to 2.5  $\mu\text{m}$ , achieved during the machining process, to 4.5–5  $\mu\text{m}$  when the vibration assistance is added into the ball burnishing process, which when it is applied alone its effect is estimated to be 3–3.5  $\mu\text{m}$  of affectation depth. Theoretically, the burnishing force and the friction force, introduced between the specimen and the tool, derivate in a significant grain size reduction due to the shearing of the process [33]. This effect is described within the external layer where the microstructure shows the characteristics of recrystallization and grain deformation in terms of  $\beta$  phase grains horizontal elongation (as it is shown in Fig. 4, 2nd and 3rd columns) or twinning and stacking-faults [34], while in the machining, these grains are bulkier and more perpendicular to the sample edge. This later with plastic deformation has stored more deformation energy, added to the fact that the dislocation

arrangement was planar and there was no cell formation, enhancing dynamic recrystallization due to the storage of elastic energy. This deformation energy is enhanced due to the vibratory effect of the assistance and can be translated into a deeper microstructure modification. Then, the main difference found between both ball burnishing processes is that vibration-assisted ball burnishing has a deeper effect compared to conventional ball burnishing, as it was also seen with other materials and the same tool-process combination [28].

### 3.3 Coefficient of friction (*cof*) analysis

The coefficient of friction evolution plots is represented in Fig. 5 for all the samples in the function of the test time. As can be seen, all the curves are characterized by three regions corresponding to the transitory (divided in ascendant and descendant slope) and steady-state. In the first one, the *cof* increases immediately due to the plastic deformation of the surface asperities and generates the track, which can be estimated during the first 5 s of the total test. Then, this coefficient is reduced dramatically and its created a friction valley that could coincide with the new microstructure that originated during the BB or VABB.

As was mentioned before, the thickness of this layer is estimated at a maximum of 5  $\mu\text{m}$  and this layer is worn during this transitory, just before entering into the bulk material and starting to stabilize. However, this valley and the later stabilization at higher *cof* values may indicate that the

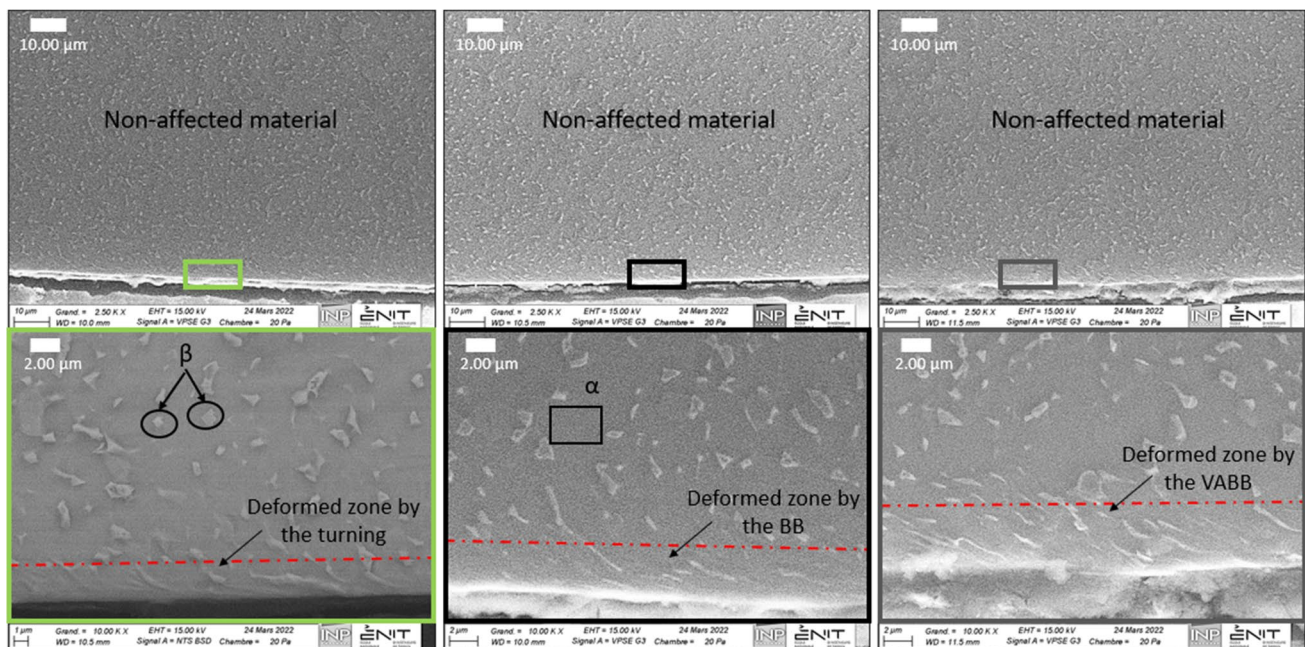


**Fig. 4** Cross-section microstructures by columns: 1st column corresponding to machined surface, 2nd column corresponding to the 130–5-0 sample (BB), and 3rd column corresponding to the 130–5-40 sample (VABB)

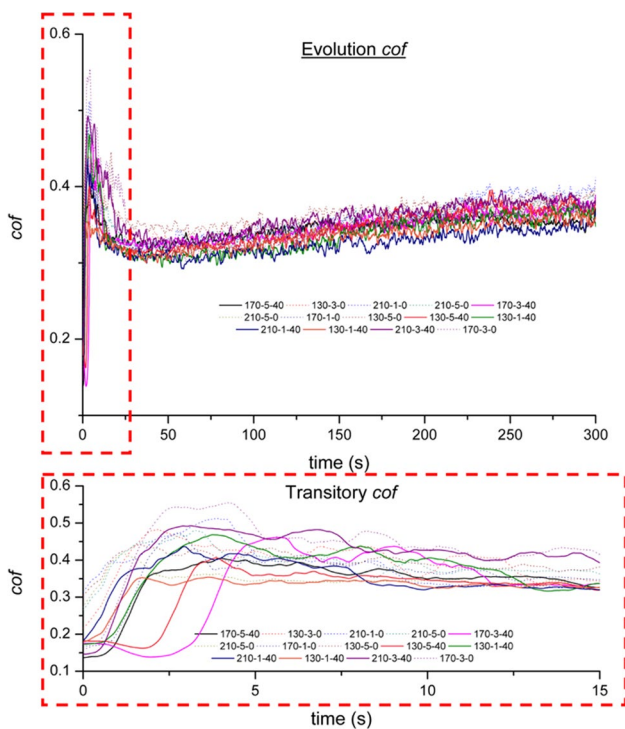


Fig. 5 Coefficient of friction steady and transitory state evolution during the test

BB/VABB process reduces the friction of the tribological system, which correlates with other investigations [35, 36].

In overall terms, the absolute analysis of the coefficient of friction (see Fig. 6) shows that there is a friction reduction of around 4.5–5% of the difference between the best and the worst performance, which indicates that the influence of the burnishing parameters is not really significant in terms of friction reduction at larger times. The best results were obtained with a combination of 210 N of force, 1 pass, and the addition of the vibration assistance, with a final value of 0.335.

### 3.4 Wear analysis

#### 3.4.1 Experimental results

The results obtained in terms of wear were more significant and conclusive than the friction results in overall terms. First of all, it was obtained the volume difference after each tribology test using a non-contact profilometer, measuring the initial and the wear track generated, superimposing them, and subtracting the difference, resulting in a volume difference in cubic micrometers. The results are presented in Fig. 7.

Figure 8a and b shows the Pareto chart and the main effects plot corresponding to the ANOVA analysis. It also calculated the interactions between all ball burnishing input

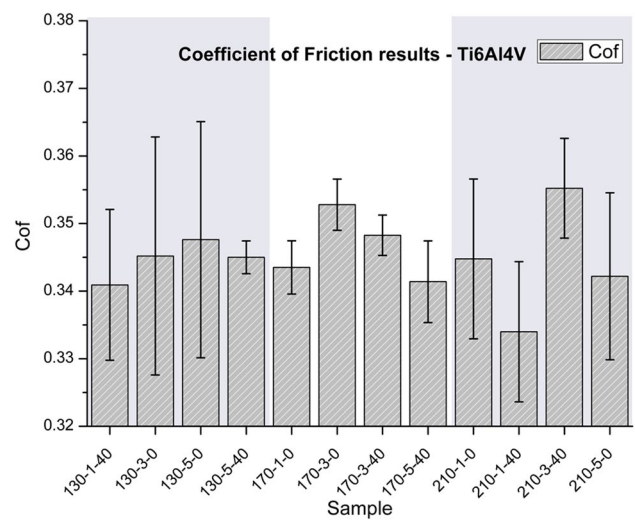


Fig. 6 Overall coefficient of friction

factors (first and second order) and the *p*-value calculation to determine the significance.

The *p*-value analysis determines that the number of passes is the most important and the only interaction with a *p*-value lower than 5%; it also noticed that the addition of the vibration assistance is close to becoming significant, having a 0.05 *p*-value; then, it could be considered that has a considerable weight on the final output wear result. In addition, the main effects plot, Fig. 8b, shows that the increase in the number of passes reduces the wear of a tribology test, which coincided with other authors [37].

The increase of force is also enhancing the wear resistance but, in this screening design, the combination of 210–5–40 was not tested and the best results were obtained with a lower force but with a combination of a

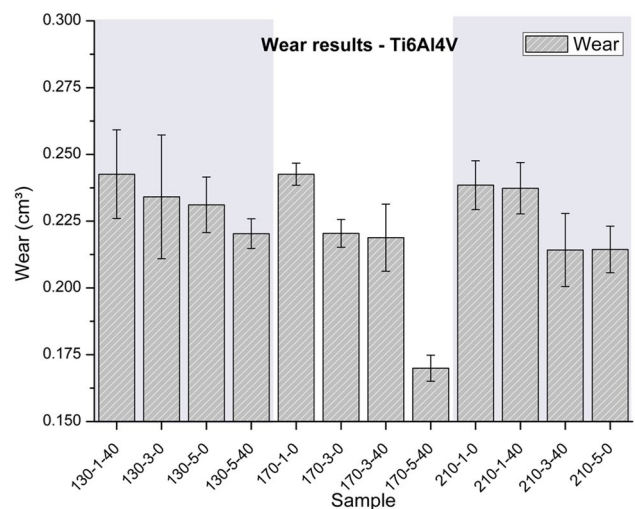
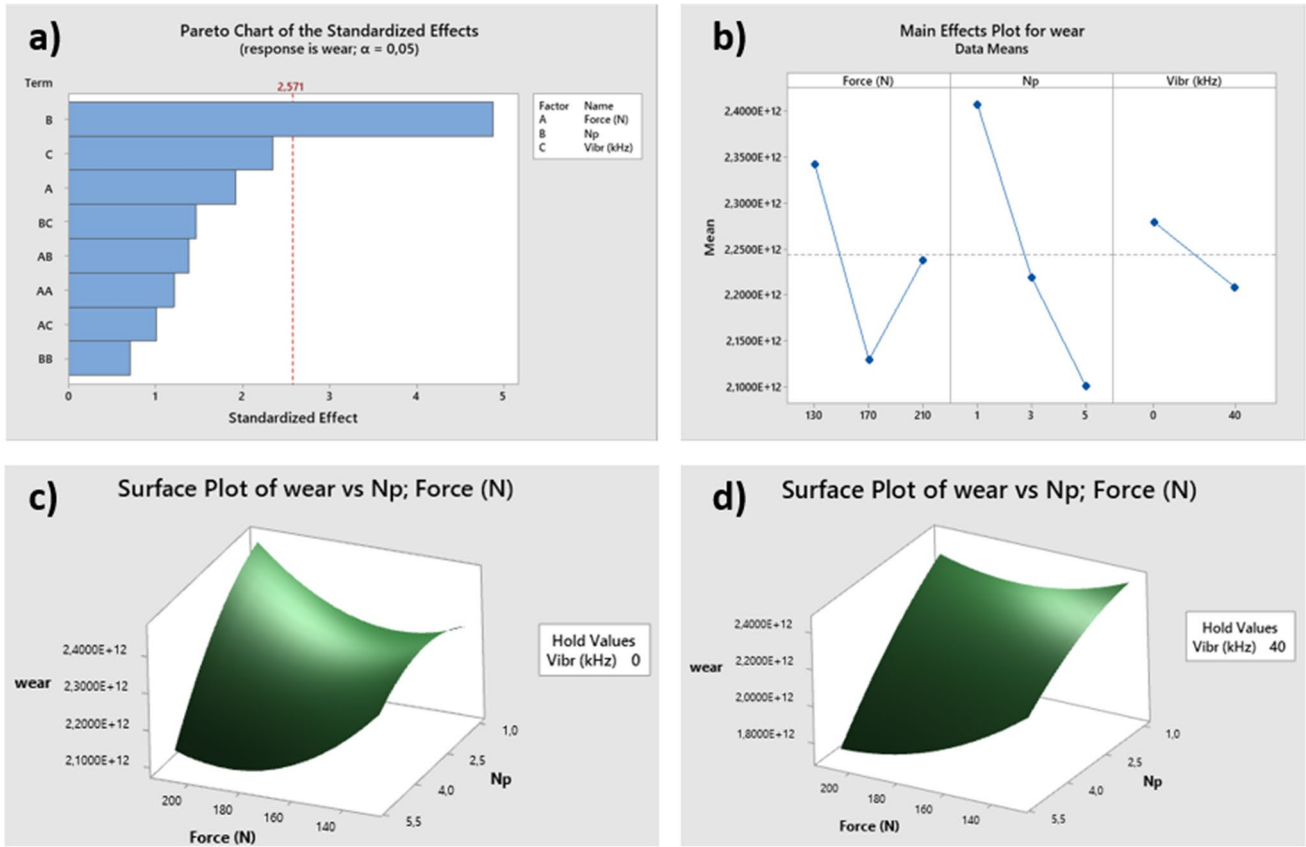


Fig. 7 Wear results for each combination



**Fig. 8** a Pareto Chart being wear as the output. b ANOVA main effect plot being wear as the. c Surface plot for BB's sample wear. d Surface plot for VABB's samples wear

high number of passes and the addition of the vibration assistance that explains the valley obtained for the force interaction. Finally, the addition of the vibration assistance is enhancing the wear resistance as can be noticed. The surface responses (see Fig. 8c and d for BB and VABB, respectively) also show a wear decrease, while the force and the number of passes are increased, but being the VABB a smoother surface and, therefore, more stable and predictable for future input parameters tuning, and complementing the behavior found through the ANOVA's analysis.

In addition, a time variation test was performed in order to determine the linearity and the variation of the wear over time. As it is shown in Fig. 9, the results show a very strong correlation with a linear interpolation but it is almost equal to a second-degree polynomial interpolation. The trend of this curve is ascendant, which means that during the first stages of the test, the surface is probably hardened and resists more the abrasion of the ball-contact cylinder, which may be related to the first layer created due to the ball burnishing process applied. Therefore, the wear resistance could be enhanced during the first tribological part, while when the bulk material layer is reached (after

2–3.5 μm, depending on the sample), the wear starts to increase, pointing that the ball burnishing could enhance the wear resistance. This hypothesis should be analyzed in deep in further investigations.

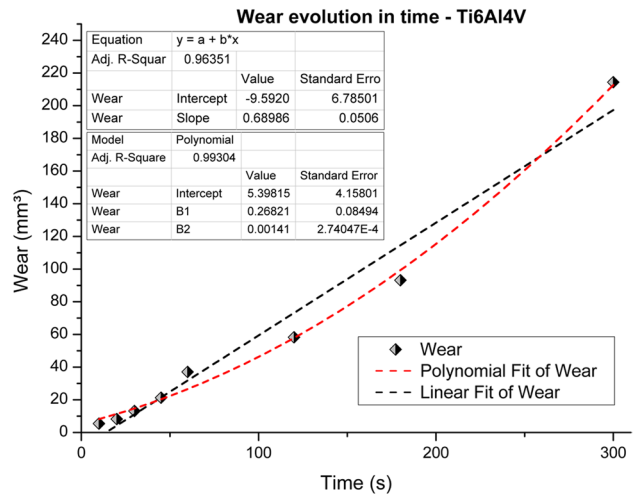


**Fig. 9** Wear evolution along the time with sample 170–3–40

### 3.4.2 Third body analysis

The visual inspections of the ball-specimen interaction were analyzed based on Berthier's accommodation modes and sites [29].

From the point of view of the ball,  $S_1$ , the only mode of accommodation found was elastic, no plastic deformation was observed, and, therefore, neither rupture, shearing, nor rolling, resulting in a mechanism  $S_1M_0$ . For the analysis of the track generated on the specimen,  $S_2$ , the material was pulled to the corners in a non-uniform way, as it showed in Fig. 10b, and forming two pile-ups and a valley, corresponding with the ball indentation and dragging effect. By analyzing the specimen worn, it is observed that the material was moved plastically but no crack growth is observed, neither shearing nor rolling, resulting in a mechanism  $S_2M_0M_1$  produced by abrasion. In addition, no material transfer is observed from the WC ball to the specimen as the EDS test revealed.

Regarding the resultant third body (see Fig. 10a), it is present a crack in the middle zone of the body that is related to the shearing produced during the repeated passes that occurred during the test, deforming and eventually cracking the contact surface. So, the resulting mechanism for the third body can be defined as  $S_3M_0M_1M_3$ .

In addition, the EDS test (see Fig. 11) on the third body surface revealed that the central part of this new body is formed by Ti, V, and Al components, which indicates the material transfer from the specimen to the ball by adhesion. It was also analyzed the oxygen presence, concluding that there is no relevance for the accommodation modes and sites by corrosion or new titanium or iron oxide formation.

## 4 Discussion

The results in terms of *cof*, during the stationary stage, of Ti6Al4V ball-burnished specimens show a very similar behavior between them and show no significant correlation against the initial surface roughness. However, in the

early stages of the test, it is shown that VABB specimens show a lower *cof* than BB specimens, showing that the vibration assistance reduces the friction force. This short effect reported could be related with the low grade of microstructure deformation, estimated at 5  $\mu\text{m}$  in the best of the cases, and a possible high input force during the tribology test. Some other authors reported that there is a relation between the surface roughness, due to the burnishing inputs applied onto the surface, and the final *cof* in Ti6Al4V specimens [12]. The *cof* is not only strongly dependent on the treated material but the counterpart's one [38] and the variability of the input load during the tribology test [39, 40] which remained constant during the experimentation. The slight difference in the *cof* values presented in this work makes it difficult to extract some conclusions due to the strong similarities between values at constant tribology inputs, so no difference when the vibration assistance is applied can be appreciated. Some more tests should be done varying the input force during the tribology or changing the counterpart's material, like stainless steels, test to analyze the effects of the VABB process on the *cof* results.

On the other hand, the number of passes was the most significant parameter in order to enhance the wear, being the vibration assistance really close to be significant enough. However, some other authors reported that the burnishing force is the most significant parameter [12]. This could be explained due to the fact that, in conventional ball burnishing, the burnishing force is required to deform the surface asperities and increase the superficial hardness. However, the increase of the number of passes could lead to a hardness increase due to the more condensed grain structure and homogeneity, which is also observed when the burnishing feed is decreased. This can be explained by the fact that the ball indenter is increasing the plastic deformation on one spot by passing several times, thus increasing the hardness. It is also known that vibration assistance increases the superficial hardness and the depth of affectation and is described as the relaxation of the quasi-static stresses, helping to deform a material and avoiding the need of exerting extra input

**Fig. 10** a Third body resultant volume. b The specimen's worn

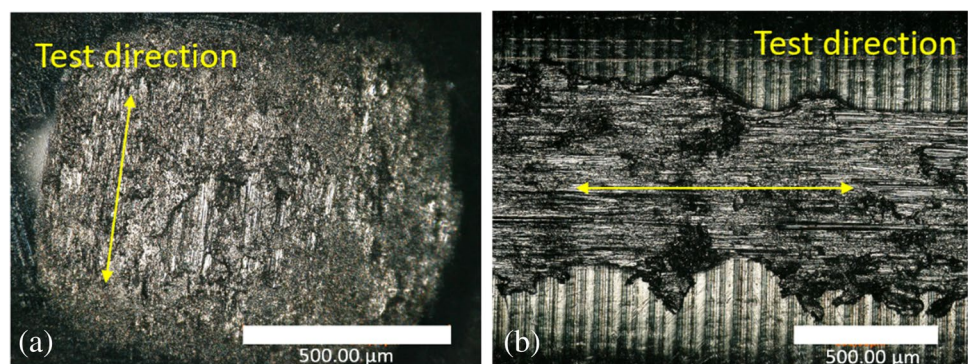
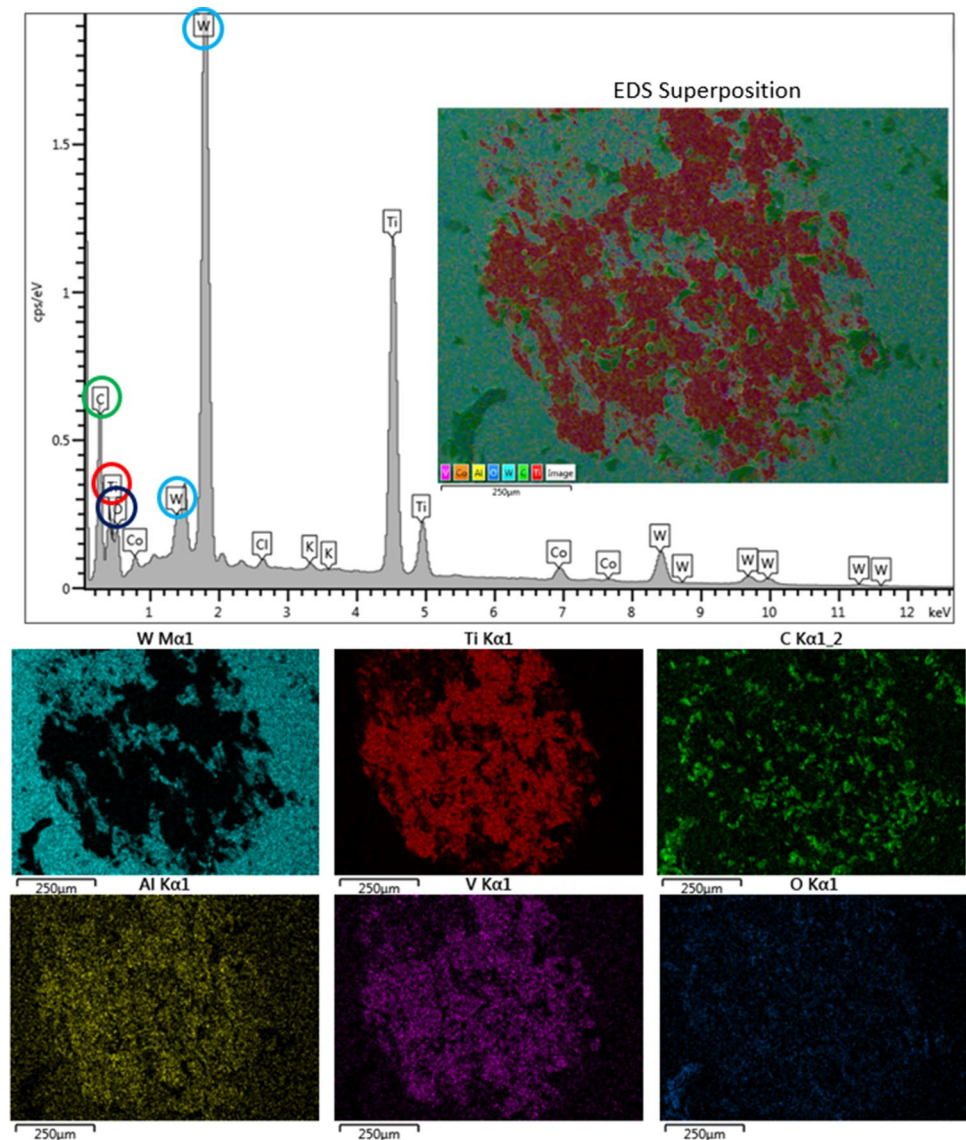


Fig. 11 EDS analysis



force. So, this combination of a high number of passes and the application of vibration assistance could lead to a new set of influential input parameters. This statement could be supported by the fact that the improvement in the surface roughness leads to a decrease in the wear [12], and it was noticed that the vibration assistance had a positive impact on roughness and wear enhancement in samples 170–5–40, 210–3–40, and 170–3–40, which share the fact of being ball burnished with vibration assistance and a medium–high level of the number of passes and burnishing force, pointing a possible relation between final surface roughness and wear.

After the presentation of these conclusions for each topic, further questions can be made regarding the effect of vibration assistance on other topological characteristics that could help to explain this phenomenology. First of all, the external hardness and the depth of affectation of this new microstructure could help to understand better

the friction and wear behavior. However, due to the thin thickness noticed at the cross-section of the samples, the measurement should be done on a nano-scale in order to measure the real effect and avoid bulk material as much as possible. Another possible future approach is to relate the wear behavior with the compressive residual stresses that originated during the burnishing process at different levels of force, the number of passes, and vibration assistance.

## 5 Conclusions

Once all results have been shown, the main conclusions of this study are as follows:

- The ball-burnishing improves the topological properties of the Ti6Al4V cylindrical surfaces, and the vibra-

tion assistance improves up to 6–10%, being a maximum roughness improvement of 70% from the initial machined surface to a vibration-assisted ball burnishing, with 210 N as the burnishing force and 3 passes in this case. The results obtained in terms of skewness and kurtosis seem very similar for all specimens.

- The vibration assistance caused an increase in the depth of this Ti6Al4V new microstructure, causing a larger deformation than the traditional ball burnishing the machining.
- The ball burnishing process seems to reduce the friction force compared to the bulk material and, more specifically, the vibration assistance seems to reduce this friction force during the 1st stage of the transitory test, which may be related to new microstructure generated by VABB/BB process, thanks to the local severe plastic deformation. However, in overall terms, the coefficient of friction seems to be similar for all conditions tested which could be directly involved in the low variation of material distribution parameters (Ssk and Sku) reported.
- The number of passes is the only significant parameter in order to enhance the wear resistance, while the vibration assistance is being to be significant enough. The evolution of the wear over time may indicate that there exists a wear reduction, while the tribological indenter is passing over the new microstructure, and increasing when the bulk material is reached.

**Author contribution** All authors contributed to the study's conception and design. Material preparation, data collection, and analysis were performed by Eric Velázquez-Corral. The first draft of the manuscript was written by Eric Velázquez-Corral, and all authors commented on previous versions of the manuscript. All authors read and approved the final manuscript.

**Funding** Open Access funding provided thanks to the CRUE-CSIC agreement with Springer Nature. Financial support for this study was provided by the Ministry of Science, Innovation and Universities of Spain, through grant RTI2018-101653-B-I00, and by the regional government of Catalonia and FEDER funds for regional development through grant IU68-016744.

**Data availability** The raw/processed data required to reproduce these findings cannot be shared at this time, as the data also forms part of an ongoing study.

**Code availability** The data that support the findings of this study are available from one of the corresponding authors, Eric Velázquez-Corral, upon reasonable request.

## Declarations

**Consent to participate** Not applicable.

**Consent for publication** The authors give consent for the publication of identifiable details, to be published in this paper.

**Conflict of interest** The authors declare no competing interests.

**Open Access** This article is licensed under a Creative Commons Attribution 4.0 International License, which permits use, sharing, adaptation, distribution and reproduction in any medium or format, as long as you give appropriate credit to the original author(s) and the source, provide a link to the Creative Commons licence, and indicate if changes were made. The images or other third party material in this article are included in the article's Creative Commons licence, unless indicated otherwise in a credit line to the material. If material is not included in the article's Creative Commons licence and your intended use is not permitted by statutory regulation or exceeds the permitted use, you will need to obtain permission directly from the copyright holder. To view a copy of this licence, visit <http://creativecommons.org/licenses/by/4.0/>.

## References

1. Hassan AM, Al-Dhifi SZ (1999) Improvement in the wear resistance of brass components by the ball burnishing process. *J Mater Process Technol* 96(1–3):73–80. [https://doi.org/10.1016/S0924-0136\(99\)00254-X](https://doi.org/10.1016/S0924-0136(99)00254-X)
2. Budinski KG (1991) Tribological properties of titanium alloys. *Wear* 151(2):203–217. [https://doi.org/10.1016/0043-1648\(91\)90249-T](https://doi.org/10.1016/0043-1648(91)90249-T)
3. Guleryuz H, Cimenoglu H (2005) Surface modification of a Ti–6Al–4V alloy by thermal oxidation. *Surf Coat Technol* 192(2–3):164–170. <https://doi.org/10.1016/j.surfcoat.2004.05.018>
4. García-Rueda AK, Guzmán-Castillo D, García-González L, Zamora-Peredo L, Hernández-Torres J (2022) Surface modification of a Ti6Al4V alloy by thermal oxidation to improve its tribological properties. *Materials Letters* 317:132082. <https://doi.org/10.1016/j.matlet.2022.132082>
5. Çakir FH, Celik ON (2020) Influence of cryogenic treatment on microstructure and mechanical properties of Ti6Al4V alloy. *J Mater Eng Perform* 29(10):6974–6984. <https://doi.org/10.1007/s11665-020-05177-y>
6. Gu K, Zhang H, Zhao B, Wang J, Zhou Y, Li Z (2013) Effect of cryogenic treatment and aging treatment on the tensile properties and micro-structure of Ti–6Al–4V alloy. *Mater Sci Eng, A* 584:170–176. <https://doi.org/10.1016/j.msea.2013.07.021>
7. Jin J, Duan H, Li X (2017) The influence of plasma nitriding on microstructure and properties of CrN and CrNiN coatings on Ti6Al4V by magnetron sputtering. *Vacuum* 136:112–120. <https://doi.org/10.1016/j.vacuum.2016.11.033>
8. Jovanović MT, Tadić S, Zec S, Mišković Z, Bobić I (2006) The effect of annealing temperatures and cooling rates on microstructure and mechanical properties of investment cast Ti–6Al–4V alloy. *Mater Des* 27(3):192–199. <https://doi.org/10.1016/j.matdes.2004.10.017>
9. Liu X, Chu PK, Ding C (2004) Surface modification of titanium, titanium alloys, and related materials for biomedical applications. *Mater Sci Eng R Rep* 47(3–4):49–121. <https://doi.org/10.1016/j.mser.2004.11.001>
10. Ganesh BKC, Sha W, Ramanaiah N, Krishnaiah A (2014) Effect of shot peening on sliding wear and tensile behavior of titanium implant alloys. *Mater Des* 1980–2015(56):480–486. <https://doi.org/10.1016/j.matdes.2013.11.052>
11. Rodríguez A, de Lacalle LL, Celaya A, Lamikiz A, Albizuri J (2012) Surface improvement of shafts by the deep ball-burnishing technique. *Surf Coat Technol* 206(11–12):2817–2824. <https://doi.org/10.1016/j.surfcoat.2011.11.045>
12. Revankar GD, Shetty R, Rao SS, Gaitonde VN (2017) Wear resistance enhancement of titanium alloy (Ti–6Al–4V) by ball

- burnishing process. *J Market Res* 6(1):13–32. <https://doi.org/10.1016/j.jmrt.2016.03.007>
13. Attabi S, Himour A, Laouar L, Motalebzadeh A (2021) Mechanical and wear behaviors of 316L stainless steel after ball burnishing treatment. *J Market Res* 15:3255–3267. <https://doi.org/10.1016/j.jmrt.2021.09.081>
  14. Tong J, Wei G, Zhao L, Wang X, Ma J (2019) Surface microstructure of titanium alloy thin-walled parts at ultrasonic vibration-assisted milling. *Int J Adv Manuf Tech* 101(1):1007–1021. <https://doi.org/10.1007/s00170-018-3005-7>
  15. Li M, Zhang Q, Han B, Song L, Cui G, Yang J, Li J (2020) Microstructure and property of Ni/WC/La<sub>2</sub>O<sub>3</sub> coatings by ultrasonic vibration-assisted laser cladding treatment. *Optics Lasers Eng* 125:105848. <https://doi.org/10.1016/j.optlaseng.2019.105848>
  16. Zhang J, Jian Y, Zhao X, Meng D, Pan F, Han Q (2021) The tribological behavior of a surface-nanocrystallized magnesium alloy AZ31 sheet after ultrasonic shot peening treatment. *J Magnes Alloys* 9(4):1187–1200. <https://doi.org/10.1016/j.jma.2020.11.012>
  17. Zhou K, Chen Y, Du ZW, Niu FL (2015) Surface integrity of titanium part by ultrasonic magnetic abrasive finishing. *Int J Adv Manuf Tech* 80(5):997–1005. <https://doi.org/10.1007/s00170-015-7028-z>
  18. Zhen-yu Z, Qiu-yang Z, Cong D, Ju-yu Y, Guang-jian P, Zhong-yu P (2021) Research on the promotion mechanism of surface burnishing process by two-dimensional ultrasonic vibration. *J Market Res* 13:1068–1082. <https://doi.org/10.1016/j.jmrt.2021.05.038>
  19. Ituarte IF, Salmi M, Papula S, Huuki J, Hemming B, Coatanea E, Virkkunen I (2020) Surface modification of additively manufactured 18% nickel maraging steel by ultrasonic vibration-assisted ball burnishing. *Journal of Manufacturing Science and Engineering* 142(7):071008. <https://doi.org/10.1115/1.4046903>
  20. Ding C, Zhou Z, Piao Z, Mao P (2022) Influence of the ultrasonic vibration on system dynamic responses in the multi-ball surface burnishing process. *J Manufac Sci Eng* 144(5):1. <https://doi.org/10.1115/1.4052392>
  21. Zhou ZY, Yu GL, Zheng QY, Ma GZ, Ye SB, Ding C, Piao ZY (2020) Wear behavior of 7075 aluminum after ultrasonic-assisted surface burnishing. *J Manuf Process* 51:1–9. <https://doi.org/10.1016/j.jmapro.2020.01.026>
  22. Amini S, Bagheri A, Teimouri R (2018) Ultrasonic-assisted ball burnishing of aluminum 6061 and AISI 1045 steel. *Mater Manuf Processes* 33(11):1250–1259. <https://doi.org/10.1080/10426914.2017.1364862>
  23. Zhang Q, Hu Z, Su W, Zhou H, Liu C, Yang Y, Qi X (2017) Microstructure and surface properties of 17–4PH stainless steel by ultrasonic surface rolling technology. *Surf Coat Technol* 321:64–73. <https://doi.org/10.1016/j.surfcoat.2017.04.052>
  24. Ren K, Yue W, Zhang H (2018) Surface modification of Ti6Al4V based on ultrasonic surface rolling processing and plasma nitriding for enhanced bone regeneration. *Surf Coat Technol* 349:602–610. <https://doi.org/10.1016/j.surfcoat.2018.06.039>
  25. Jerez-Mesa R, Travieso-Rodríguez JA, Landon Y, Dessein G, Lluma-Fuentes J, Wagner V (2019) Comprehensive analysis of surface integrity modification of ball-end milled Ti-6Al-4V surfaces through vibration-assisted ball burnishing. *J Mater Process Technol* 267:230–240. <https://doi.org/10.1016/j.jmatprotec.2018.12.022>
  26. Teimouri R, Amini S, Bami AB (2018) Evaluation of optimized surface properties and residual stress in ultrasonic assisted ball burnishing of AA6061-T6. *Measurement* 116:129–139. <https://doi.org/10.1016/j.measurement.2017.11.001>
  27. Liu Y, Wang L, Wang D (2011) Finite element modeling of ultrasonic surface rolling process. *J Mater Process Technol* 211(12):2106–2113. <https://doi.org/10.1016/j.jmatprotec.2011.07.009>
  28. Velázquez-Corral E, Jerez-Mesa R, Llumà J, Wagner V, Dessein G, Travieso-Rodríguez JA (2022) Wear resistance enhancement of AISI 1045 steel by vibration assisted ball burnishing process. *Procedia CIRP* 108:287–292. <https://doi.org/10.1016/j.procir.2022.03.049>
  29. Berthier Y, Godet M, Brendle M (1989) Velocity accommodation in friction. *Tribology Transactions* 32(4):490–496. <https://doi.org/10.1080/10402008908981917>
  30. Godet M (1984) The third-body approach: a mechanical view of wear. *Wear* 100(1–3):437–452. [https://doi.org/10.1016/0043-1648\(84\)90025-5](https://doi.org/10.1016/0043-1648(84)90025-5)
  31. Denape, J. (2015). Third body concept and wear particle behavior in dry friction sliding conditions. In *Key Engineering Materials* (Vol. 640, pp. 1–12). Trans Tech Publications Ltd. <https://doi.org/10.4028/www.scientific.net/KEM.640>.
  32. Ba, Elhadji Cheikh Talibouya, et al. Investigation of the effects of skewness R<sub>sk</sub> and kurtosis R<sub>ku</sub> on tribological behavior in a pin-on-disc test of surfaces machined by conventional milling and turning processes. *Materials Research* 24 (2021). <https://doi.org/10.1590/1980-5373-MR-2020-0435>
  33. Rotella G, Rinaldi S, Filice L (2020) Roller burnishing of Ti6Al4V under different cooling/lubrication conditions and tool design: effects on surface integrity. *Int J Adv Manuf Tech* 106(1):431–440. <https://doi.org/10.1007/s00170-019-04631-z>
  34. Wu X, Tao N, Hong Y, Liu G, Xu B, Lu J, Lu KJAM (2005) Strain-induced grain refinement of cobalt during surface mechanical attrition treatment. *Acta Mater* 53(3):681–691. <https://doi.org/10.1016/j.actamat.2004.10.021>
  35. El-Tayeb NSM, Low KO, Brevern PV (2008) Enhancement of surface quality and tribological properties using ball burnishing process. *Mach Sci Technol* 12(2):234–248. <https://doi.org/10.1080/10910340802067536>
  36. Dzierwa A, Markopoulos AP (2019) Influence of ball-burnishing process on surface topography parameters and tribological properties of hardened steel. *Machines* 7(1):11. <https://doi.org/10.3390/machines7010011>
  37. Mahajan D, Tajane R (2013) A review on ball burnishing process. *Int J Sci Res Publ* 3(4):1–8
  38. Dong H, Shi W, Bell T (1999) Potential of improving tribological performance of UHMWPE by engineering the Ti6Al4V counterfaces. *Wear* 225:146–153. [https://doi.org/10.1016/S0043-1648\(98\)00356-1](https://doi.org/10.1016/S0043-1648(98)00356-1)
  39. Niu Q, Zheng X, Chen M, Ming W (2014) Study on the tribological properties of titanium alloys sliding against WC-Co during the dry friction. *Ind Lubr Tribol*. <https://doi.org/10.1108/ILT-11-2011-0099>
  40. Zhao W, He N, Li L (2011) Friction and wear properties of WC-Co cemented carbide sliding against Ti6Al4V alloy in nitrogen gas. *Adv Mater Res* 188:49–54. <https://doi.org/10.4028/www.scientific.net/AMR.188.49>

**Publisher's note** Springer Nature remains neutral with regard to jurisdictional claims in published maps and institutional affiliations.